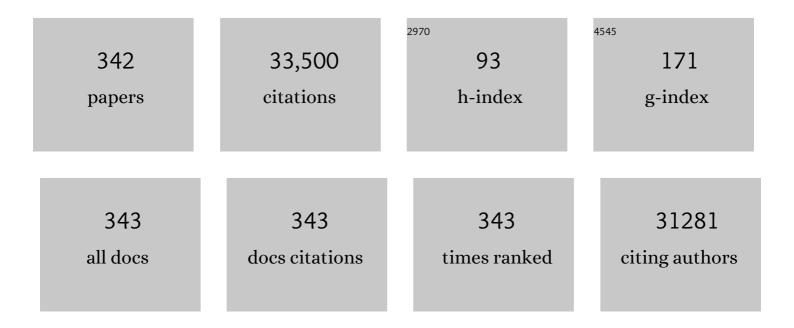
Taihong Wang

List of Publications by Year in descending order

Source: https://exaly.com/author-pdf/9474919/publications.pdf Version: 2024-02-01



#	Article	IF	CITATIONS
1	Intrinsic peroxidase-like activity of ferromagnetic nanoparticles. Nature Nanotechnology, 2007, 2, 577-583.	15.6	5,080
2	Fabrication and ethanol sensing characteristics of ZnO nanowire gas sensors. Applied Physics Letters, 2004, 84, 3654-3656.	1.5	1,869
3	Layered SnS ₂ â€Reduced Graphene Oxide Composite – A Highâ€Capacity, Highâ€Rate, and Longâ€Cycle Life Sodiumâ€Ion Battery Anode Material. Advanced Materials, 2014, 26, 3854-3859.	11.1	744
4	Adsorption and desorption of oxygen probed from ZnO nanowire films by photocurrent measurements. Applied Physics Letters, 2005, 86, 123117.	1.5	452
5	Positive Potential Operation of a Cathodic Electrogenerated Chemiluminescence Immunosensor Based on Luminol and Graphene for Cancer Biomarker Detection. Analytical Chemistry, 2011, 83, 3817-3823.	3.2	347
6	Oxygen sensing characteristics of individual ZnO nanowire transistors. Applied Physics Letters, 2004, 85, 6389-6391.	1.5	338
7	A novel nonenzymatic hydrogen peroxide sensor based on MnO2/graphene oxide nanocomposite. Talanta, 2010, 82, 1637-1641.	2.9	320
8	Nanomaterials for electrochemical non-enzymatic glucose biosensors. RSC Advances, 2013, 3, 3487.	1.7	315
9	High performance NiMoO4 nanowires supported on carbon cloth as advanced electrodes for symmetric supercapacitors. Nano Energy, 2014, 8, 174-182.	8.2	301
10	Low-field electron emission from tetrapod-like ZnO nanostructures synthesized by rapid evaporation. Applied Physics Letters, 2003, 83, 2253-2255.	1.5	300
11	Synthesis and properties of multipod-shaped ZnO nanorods for gas-sensor applications. Applied Physics A: Materials Science and Processing, 2005, 80, 1451-1454.	1.1	290
12	Magnetite/graphene composites: microwave irradiation synthesis and enhanced cycling and rate performances for lithium ion batteries. Journal of Materials Chemistry, 2010, 20, 5538.	6.7	284
13	Flexible ReS2 nanosheets/N-doped carbon nanofibers-based paper as a universal anode for alkali (Li, Na,) Tj ETQq1	1,0.7843 8.2	14 rgBT /Ov
14	Nanoforest of hierarchical Co3O4@NiCo2O4 nanowire arrays for high-performance supercapacitors. Nano Energy, 2013, 2, 586-594.	8.2	278
15	Sonochemical Synthesis, Optical Properties, and Electrical Properties of Core/Shell-Type ZnO Nanorod/CdS Nanoparticle Composites. Chemistry of Materials, 2005, 17, 887-892.	3.2	272
16	Pipe-Wire TiO ₂ –Sn@Carbon Nanofibers Paper Anodes for Lithium and Sodium Ion Batteries. Nano Letters, 2017, 17, 3830-3836.	4.5	272
17	Electronic transport through individual ZnO nanowires. Applied Physics Letters, 2004, 84, 4556-4558.	1.5	270
18	Comparison of the Electrochemical Performance of NiMoO ₄ Nanorods and Hierarchical Nanospheres for Supercapacitor Applications. ACS Applied Materials & Interfaces, 2013, 5, 12905-12910.	4.0	267

#	Article	IF	CITATIONS
19	Hierarchical mushroom-like CoNi2S4 arrays as a novel electrode material for supercapacitors. Nano Energy, 2014, 3, 36-45.	8.2	265
20	Contact-controlled sensing properties of flowerlike ZnO nanostructures. Applied Physics Letters, 2005, 87, 213111.	1.5	263
21	Ultrathin Porous NiCo ₂ O ₄ Nanosheet Arrays on Flexible Carbon Fabric for High-Performance Supercapacitors. ACS Applied Materials & Interfaces, 2013, 5, 7405-7409.	4.0	259
22	Synthesis and H ₂ S Sensing Properties of CuOâ^'SnO ₂ Core/Shell PN-Junction Nanorods. Journal of Physical Chemistry C, 2008, 112, 12157-12160.	1.5	258
23	One-Step Synthesis of Hierarchical SnO ₂ Hollow Nanostructures via Self-Assembly for High Power Lithium Ion Batteries. Journal of Physical Chemistry C, 2010, 114, 8084-8088.	1.5	258
24	Synthesis, Self-Assembly, Disassembly, and Reassembly of Two Types of Cu ₂ 0 Nanocrystals Unifaceted with {001} or {110} Planes. Journal of the American Chemical Society, 2010, 132, 6131-6144.	6.6	251
25	Facile synthesis of uniform mesoporous ZnCo2O4 microspheres as a high-performance anode material for Li-ion batteries. Journal of Materials Chemistry A, 2013, 1, 5596.	5.2	250
26	Facile synthesis and excellent electrochemical properties of CoMoO4 nanoplate arrays as supercapacitors. Journal of Materials Chemistry A, 2013, 1, 7247.	5.2	246
27	High-performance supercapacitor and lithium-ion battery based on 3D hierarchical NH4F-induced nickel cobaltate nanosheet–nanowire cluster arrays as self-supported electrodes. Nanoscale, 2013, 5, 9812.	2.8	242
28	Microwave absorption properties of the ZnO nanowire-polyester composites. Applied Physics Letters, 2004, 84, 3367-3369.	1.5	225
29	Controllable Fabrication and Electrical Performance of Single Crystalline Cu ₂ O Nanowires with High Aspect Ratios. Nano Letters, 2007, 7, 3723-3728.	4.5	225
30	Metastable Vanadium Dioxide Nanobelts: Hydrothermal Synthesis, Electrical Transport, and Magnetic Properties. Angewandte Chemie - International Edition, 2004, 43, 5048-5052.	7.2	214
31	Synthesis and ethanol sensing characteristics of single crystalline SnO2 nanorods. Applied Physics Letters, 2005, 87, 233503.	1.5	212
32	High-Performance Supercapacitor Electrode Based on the Unique ZnO@Co ₃ O ₄ Core/Shell Heterostructures on Nickel Foam. ACS Applied Materials & Interfaces, 2014, 6, 15905-15912.	4.0	212
33	Construction of desirable NiCo2S4 nanotube arrays on nickel foam substrate for pseudocapacitors with enhanced performance. Electrochimica Acta, 2015, 151, 35-41.	2.6	206
34	Fast synthesis of SnO2/graphene composites by reducing graphene oxide with stannous ions. Journal of Materials Chemistry, 2011, 21, 1673-1676.	6.7	201
35	Enhanced Sensitivity and Stability of Room-Temperature NH ₃ Sensors Using Core–Shell CeO ₂ Nanoparticles@Cross-linked PANI with p–n Heterojunctions. ACS Applied Materials & Interfaces, 2014, 6, 14131-14140.	4.0	201
36	Three-Dimensional Co ₃ O ₄ @NiMoO ₄ Core/Shell Nanowire Arrays on Ni Foam for Electrochemical Energy Storage. ACS Applied Materials & Interfaces, 2014, 6, 5050-5055.	4.0	198

#	Article	IF	CITATIONS
37	Low-resistance gas sensors fabricated from multiwalled carbon nanotubes coated with a thin tin oxide layer. Applied Physics Letters, 2004, 85, 666-668.	1.5	195
38	CdS nanobelts as photoconductors. Applied Physics Letters, 2005, 86, 173105.	1.5	194
39	Morphogenesis of Highly Uniform CoCO ₃ Submicrometer Crystals and Their Conversion to Mesoporous Co ₃ O ₄ for Gas-Sensing Applications. Chemistry of Materials, 2009, 21, 4984-4992.	3.2	194
40	Individual β-Ga2O3 nanowires as solar-blind photodetectors. Applied Physics Letters, 2006, 88, 153107.	1.5	192
41	Room-temperature hydrogen storage characteristics of ZnO nanowires. Applied Physics Letters, 2004, 84, 124-126.	1.5	186
42	NiMoO4 nanowires supported on Ni foam as novel advanced electrodes for supercapacitors. Journal of Materials Chemistry A, 2013, 1, 9024.	5.2	185
43	A novel amperometric biosensor based on NiO hollow nanospheres for biosensing glucose. Talanta, 2008, 77, 455-459.	2.9	176
44	Electrochemical performance of polycrystalline CuO nanowires as anode material for Li ion batteries. Electrochimica Acta, 2009, 54, 4198-4201.	2.6	175
45	Electrospun porous SnO2 nanotubes as high capacity anode materials for lithium ion batteries. Electrochemistry Communications, 2010, 12, 1383-1386.	2.3	174
46	The structure control of ZnS/graphene composites and their excellent properties for lithium-ion batteries. Journal of Materials Chemistry A, 2015, 3, 13384-13389.	5.2	172
47	The enhanced ethanol sensing properties of multi-walled carbon nanotubes/SnO2core/shell nanostructures. Nanotechnology, 2006, 17, 3012-3017.	1.3	169
48	Positive temperature coefficient resistance and humidity sensing properties of Cd-doped ZnO nanowires. Applied Physics Letters, 2004, 84, 3085-3087.	1.5	161
49	Simple method for the preparation of highly porous ZnCo2O4 nanotubes with enhanced electrochemical property for supercapacitor. Electrochimica Acta, 2014, 123, 450-455.	2.6	160
50	High Sulfur Loading in Hierarchical Porous Carbon Rods Constructed by Vertically Oriented Porous Graphene‣ike Nanosheets for Li‧ Batteries. Advanced Functional Materials, 2016, 26, 8952-8959.	7.8	159
51	Carbon Nanotube Delivery of the GFP Gene into Mammalian Cells. ChemBioChem, 2006, 7, 239-242.	1.3	156
52	Plate-like p–n heterogeneous NiO/WO3 nanocomposites for high performance room temperature NO2 sensors. Nanoscale, 2014, 6, 4063.	2.8	155
53	CoO–carbon nanofiber networks prepared by electrospinning as binder-free anode materials for lithium-ion batteries with enhanced properties. Nanoscale, 2013, 5, 12342.	2.8	149
54	Ab Initio Study of ZnO-Based Gas-Sensing Mechanisms: Surface Reconstruction and Charge Transfer. Journal of Physical Chemistry C, 2009, 113, 6107-6113.	1.5	147

#	Article	IF	CITATIONS
55	In situ synthesis of SnO2/graphene nanocomposite and their application as anode material for lithium ion battery. Materials Letters, 2010, 64, 2076-2079.	1.3	146
56	Highly Sensitive Electrogenerated Chemiluminescence Biosensor in Profiling Protein Kinase Activity and Inhibition Using Gold Nanoparticle as Signal Transduction Probes. Analytical Chemistry, 2010, 82, 9566-9572.	3.2	145
57	β-Cobalt sulfide nanoparticles decorated graphene composite electrodes for high capacity and power supercapacitors. Nanoscale, 2012, 4, 7810.	2.8	145
58	An amorphous Si thin film anode with high capacity and long cycling life for lithium ion batteries. Journal of Applied Electrochemistry, 2009, 39, 1157-1162.	1.5	142
59	Stable field emission from tetrapod-like ZnO nanostructures. Applied Physics Letters, 2004, 85, 636-638.	1.5	139
60	Porous Carbon Nanofibers Derived from Conducting Polymer: Synthesis and Application in Lithium-Ion Batteries with High-Rate Capability. Journal of Physical Chemistry C, 2009, 113, 13438-13442.	1.5	139
61	Topochemical Preparation of WO ₃ Nanoplates through Precursor H ₂ WO ₄ and Their Gas-Sensing Performances. Journal of Physical Chemistry C, 2011, 115, 18157-18163.	1.5	137
62	High-Performance Lithium-Ion Battery Anode by Direct Growth of Hierarchical ZnCo ₂ O ₄ Nanostructures on Current Collectors. ACS Applied Materials & Interfaces, 2014, 6, 731-736.	4.0	137
63	Low-Temperature H ₂ S Detection with Hierarchical Cr-Doped WO ₃ Microspheres. ACS Applied Materials & Interfaces, 2016, 8, 9674-9683.	4.0	136
64	Facile solvothermal synthesis of mesoporous Cu2SnS3 spheres and their application in lithium-ion batteries. Nanoscale, 2011, 3, 3646.	2.8	135
65	Construction of unique NiCo2O4 nanowire@CoMoO4 nanoplate core/shell arrays on Ni foam for high areal capacitance supercapacitors. Journal of Materials Chemistry A, 2014, 2, 4954.	5.2	134
66	Synthesis of Cobalt Ionâ€Based Coordination Polymer Nanowires and Their Conversion into Porous Co ₃ O ₄ Nanowires with Good Lithium Storage Properties. Chemistry - A European Journal, 2010, 16, 5215-5221.	1.7	131
67	Reduced graphene oxide networks as an effective buffer matrix to improve the electrode performance of porous NiCo2O4 nanoplates for lithium-ion batteries. Journal of Materials Chemistry A, 2014, 2, 4449.	5.2	131
68	Fast humidity sensors based on CeO2nanowires. Nanotechnology, 2007, 18, 145503.	1.3	130
69	Synthesis of Bacteria Promoted Reduced Graphene Oxide-Nickel Sulfide Networks for Advanced Supercapacitors. ACS Applied Materials & amp; Interfaces, 2013, 5, 7335-7340.	4.0	130
70	Synthesis and ethanol sensing properties of ZnSnO3 nanowires. Applied Physics Letters, 2005, 86, 233101.	1.5	127
71	A green and fast strategy for the scalable synthesis of Fe2O3/graphene with significantly enhanced Li-ion storage properties. Journal of Materials Chemistry, 2012, 22, 3868.	6.7	125
72	Three-Dimensional Functionalized Tetrapod-like ZnO Nanostructures for Plasmid DNA Delivery. Small, 2006, 2, 621-625.	5.2	124

#	Article	IF	CITATIONS
73	Targeting Chemophotothermal Therapy of Hepatoma by Gold Nanorods/Graphene Oxide Core/Shell Nanocomposites. ACS Applied Materials & Interfaces, 2013, 5, 12911-12920.	4.0	123
74	Ultralong Singleâ€Crystalline Ag ₂ S Nanowires: Promising Candidates for Photoswitches and Roomâ€Temperature Oxygen Sensors. Advanced Materials, 2008, 20, 2628-2632.	11.1	121
75	Flexible CoO–graphene–carbon nanofiber mats as binder-free anodes for lithium-ion batteries with superior rate capacity and cyclic stability. Journal of Materials Chemistry A, 2014, 2, 5890-5897.	5.2	121
76	Construction of hierarchical CoS nanowire@NiCo ₂ S ₄ nanosheet arrays via one-step ion exchange for high-performance supercapacitors. Journal of Materials Chemistry A, 2015, 3, 24033-24040.	5.2	119
77	Surface accumulation conduction controlled sensing characteristic of p-type CuO nanorods induced by oxygen adsorption. Nanotechnology, 2007, 18, 145506.	1.3	118
78	Enhanced performance of supercapacitors with ultrathin mesoporous NiMoO4 nanosheets. Electrochimica Acta, 2014, 125, 294-301.	2.6	116
79	One-Step Synthesis and Gas-Sensing Characteristics of Uniformly Loaded Pt@SnO ₂ Nanorods. Journal of Physical Chemistry C, 2010, 114, 3968-3972.	1.5	115
80	Facile synthesis of carbon nanofibers/MnO2 nanosheets as high-performance electrodes for asymmetric supercapacitors. Electrochimica Acta, 2016, 210, 754-761.	2.6	115
81	Field-emission from long SnO2 nanobelt arrays. Applied Physics Letters, 2004, 85, 5682-5684.	1.5	113
82	Superior electrochemical performance of ultrasmall SnS2 nanocrystals decorated on flexible RGO in lithium-ion batteries. Journal of Materials Chemistry A, 2013, 1, 8658.	5.2	110
83	Facile hydrothermal synthesis of hierarchical ultrathin mesoporous NiMoO4 nanosheets for high performance supercapacitors. Electrochimica Acta, 2014, 115, 358-363.	2.6	110
84	Porous platelike hematite mesocrystals: synthesis, catalytic and gas-sensing applications. Journal of Materials Chemistry, 2012, 22, 11694.	6.7	109
85	α-Fe ₂ O ₃ nanochains: ammonium acetate-based ionothermal synthesis and ultrasensitive sensors for low-ppm-level H ₂ S gas. Nanoscale, 2013, 5, 895-898.	2.8	107
86	Enhanced gas sensing properties of ZnO/SnO ₂ hierarchical architectures by glucose-induced attachment. CrystEngComm, 2011, 13, 1557-1563.	1.3	105
87	Branched SnO2 nanowires on metallic nanowire backbones for ethanol sensors application. Applied Physics Letters, 2008, 92, .	1.5	103
88	Catalyst-Assisted Vaporâ^'Liquidâ^'Solid Growth of Single-Crystal CdS Nanobelts and Their Luminescence Properties. Journal of Physical Chemistry B, 2004, 108, 20045-20049.	1.2	102
89	Synthesis and ethanol sensing properties of indium-doped tin oxide nanowires. Applied Physics Letters, 2006, 88, 201907.	1.5	101
90	Flexible morphology-controlled synthesis of mesoporous hierarchical α-Fe2O3 architectures and their gas-sensing properties. CrystEngComm, 2011, 13, 806-812.	1.3	100

#	Article	IF	CITATIONS
91	Growth of NiCo ₂ O ₄ @MnMoO ₄ Nanocolumn Arrays with Superior Pseudocapacitor Properties. ACS Applied Materials & Interfaces, 2016, 8, 8568-8575.	4.0	100
92	Black phosphorus-based van der Waals heterostructures for mid-infrared light-emission applications. Light: Science and Applications, 2020, 9, 114.	7.7	100
93	Graphene oxide oxidizes stannous ions to synthesize tin sulfide–graphene nanocomposites with small crystal size for high performance lithium ion batteries. Journal of Materials Chemistry, 2012, 22, 23091.	6.7	97
94	Synthesis of mesoporous NiO nanospheres as anode materials for lithium ion batteries. Electrochimica Acta, 2012, 80, 140-147.	2.6	95
95	Metal–organic-framework-derived ZnO@C@NiCo ₂ O ₄ core–shell structures as an advanced electrode for high-performance supercapacitors. Journal of Materials Chemistry A, 2016, 4, 8233-8241.	5.2	94
96	Promises and challenges of tin-based compounds as anode materials for lithium-ion batteries. International Materials Reviews, 2015, 60, 330-352.	9.4	93
97	α-Fe2O3 nanowall arrays: hydrothermal preparation, growth mechanism and excellent rate performances for lithium ion batteries. Nanoscale, 2012, 4, 3422.	2.8	92
98	Enhanced electrochemical performance of CoMoO4 nanorods/reduced graphene oxide as anode material for lithium-ion batteries. Electrochimica Acta, 2015, 158, 327-332.	2.6	92
99	Synthesis of ZnSnO3 mesocrystals from regular cube-like to sheet-like structures and their comparative electrochemical properties in Li-ion batteries. Journal of Materials Chemistry, 2012, 22, 25373.	6.7	91
100	Superior ethanol-sensing properties based on Ni-doped SnO2 p–n heterojunction hollow spheres. Sensors and Actuators B: Chemical, 2012, 166-167, 61-67.	4.0	90
101	Preparation of 3D flower-like NiO hierarchical architectures and their electrochemical properties in lithium-ion batteries. Electrochimica Acta, 2013, 90, 80-89.	2.6	90
102	Construction of 3D flower-like MoS2 spheres with nanosheets as anode materials for high-performance lithium ion batteries. Electrochimica Acta, 2014, 115, 165-169.	2.6	90
103	High performance and negative temperature coefficient of low temperature hydrogen gas sensors using palladium decorated tungsten oxide. Journal of Materials Chemistry A, 2015, 3, 1317-1324.	5.2	90
104	Sonochemical synthesis of SnO2 nanobelt/CdS nanoparticle core/shell heterostructures. Chemical Communications, 2004, , 2558.	2.2	89
105	Encapsulating Gold Nanoparticles or Nanorods in Graphene Oxide Shells as a Novel Gene Vector. ACS Applied Materials & Interfaces, 2013, 5, 2715-2724.	4.0	89
106	Porous α-Fe2O3 nanosphere-based H2S sensor with fast response, high selectivity and enhanced sensitivity. Journal of Materials Chemistry A, 2013, 1, 12400.	5.2	89
107	Morphology controlled synthesis of NiCo 2 O 4 nanosheet array nanostructures on nickel foam and their application for pseudocapacitors. Electrochimica Acta, 2014, 142, 118-124.	2.6	88
108	Rapid and ultrahigh ethanol sensing based on Au-coated ZnO nanorods. Nanotechnology, 2008, 19, 035501.	1.3	86

#	Article	IF	CITATIONS
109	Synthesis of self-assembled 3D flowerlike SnS2 nanostructures with enhanced lithium ion storage property. Solid State Sciences, 2010, 12, 712-718.	1.5	86
110	SnO ₂ monolayer porous hollow spheres as a gas sensor. Nanotechnology, 2009, 20, 455503.	1.3	85
111	Carbon and graphene double protection strategy to improve the SnOx electrode performance anodes for lithium-ion batteries. Nanoscale, 2013, 5, 5499.	2.8	85
112	Plate-like SnS ₂ nanostructures: Hydrothermal preparation, growth mechanism and excellent electrochemical properties. CrystEngComm, 2012, 14, 832-836.	1.3	84
113	Hierarchical Mo-decorated Co3O4 nanowire arrays on Ni foam substrates for advanced electrochemical capacitors. Journal of Materials Chemistry A, 2013, 1, 8593.	5.2	84
114	High-temperature humidity sensors based on WO ₃ –SnO ₂ composite hollow nanospheres. Journal of Materials Chemistry A, 2014, 2, 6854-6862.	5.2	84
115	High-performance ethanol sensing based on an aligned assembly of ZnO nanorods. Sensors and Actuators B: Chemical, 2008, 135, 57-60.	4.0	83
116	Ternary Cu2SnS3 cabbage-like nanostructures: large-scale synthesis and their application in Li-ion batteries with superior reversible capacity. Nanoscale, 2011, 3, 4389.	2.8	83
117	WO3 nanoparticles decorated on both sidewalls of highly porous TiO2 nanotubes to improve UV and visible-light photocatalysis. Journal of Materials Chemistry A, 2013, 1, 3900.	5.2	82
118	Shot Noise with Interaction Effects in Single-Walled Carbon Nanotubes. Physical Review Letters, 2007, 99, 156803.	2.9	81
119	Improved room-temperature hydrogen sensing performance of directly formed Pd/WO3 nanocomposite. Sensors and Actuators B: Chemical, 2014, 193, 28-34.	4.0	81
120	1D Nb-doped LiNi1/3Co1/3Mn1/3O2 nanostructures as excellent cathodes for Li-ion battery. Electrochimica Acta, 2019, 297, 258-266.	2.6	81
121	Giant negative thermopower of ionic hydrogel by synergistic coordination and hydration interactions. Science Advances, 2021, 7, eabi7233.	4.7	81
122	NiO nanomaterials: controlled fabrication, formation mechanism and the application in lithium-ion battery. CrystEngComm, 2012, 14, 453-459.	1.3	79
123	High electrochemical performance based on the TiO ₂ nanobelt@few-layered MoS ₂ structure for lithium-ion batteries. Nanoscale, 2014, 6, 12350-12353.	2.8	78
124	Rational synthesis of metal–organic framework composites, hollow structures and their derived porous mixed metal oxide hollow structures. Journal of Materials Chemistry A, 2016, 4, 183-192.	5.2	77
125	Achieving fast oxygen response in individual β-Ga2O3 nanowires by ultraviolet illumination. Applied Physics Letters, 2006, 89, 112114.	1.5	76
126	Porous NiCo2O4-reduced graphene oxide (rGO) composite with superior capacitance retention for supercapacitors. Electrochimica Acta, 2014, 132, 332-337.	2.6	76

#	Article	IF	CITATIONS
127	Facile synthesis of well-ordered manganese oxide nanosheet arrays on carbon cloth for high-performance supercapacitors. Journal of Materials Chemistry A, 2014, 2, 8833.	5.2	76
128	Enhanced Optical and Sensing Properties of One-Step Synthesized Ptâ^'ZnO Nanoflowers. Journal of Physical Chemistry C, 2010, 114, 18607-18611.	1.5	74
129	An evolution from 3D face-centered-cubic ZnSnO ₃ nanocubes to 2D orthorhombic ZnSnO ₃ nanosheets with excellent gas sensing performance. Nanotechnology, 2012, 23, 415501.	1.3	73
130	Single Nozzle Electrospinning Synthesized MoO ₂ @C Core Shell Nanofibers with High Capacity and Longâ€Term Stability for Lithiumâ€Ion Storage. Advanced Materials Interfaces, 2017, 4, 1600816.	1.9	73
131	Bandgap narrowing and ethanol sensing properties of In-doped ZnO nanowires. Nanotechnology, 2007, 18, 225504.	1.3	72
132	Si–Al thin film anode material with superior cycle performance and rate capability for lithium ion batteries. Electrochimica Acta, 2008, 53, 8149-8153.	2.6	71
133	Enhanced selective acetone sensing characteristics based on Co-doped WO3 hierarchical flower-like nanostructures assembled with nanoplates. Sensors and Actuators B: Chemical, 2016, 235, 614-621.	4.0	70
134	Optoelectronic characteristics of single CdS nanobelts. Applied Physics Letters, 2005, 86, 193109.	1.5	68
135	Room-temperature hydrogen sensor based on grain-boundary controlled Pt decorated In2O3 nanocubes. Sensors and Actuators B: Chemical, 2014, 201, 351-359.	4.0	68
136	High performance humidity sensors based on CeO2 nanoparticles. Sensors and Actuators B: Chemical, 2015, 215, 125-132.	4.0	67
137	Vertically aligned tin-doped indium oxide nanowire arrays: Epitaxial growth and electron field emission properties. Applied Physics Letters, 2006, 89, 123102.	1.5	66
138	Bi2S3 nanomaterials: morphology manipulation and related properties. Dalton Transactions, 2011, 40, 10100.	1.6	66
139	Synthesis of mesoporous SnO2 spheres via self-assembly and superior lithium storage properties. Electrochimica Acta, 2011, 56, 2358-2363.	2.6	66
140	A Facile Titanium Glycolate Precursor Route to Mesoporous Au/Li ₄ Ti ₅ O ₁₂ Spheres for High-Rate Lithium-Ion Batteries. ACS Applied Materials & Interfaces, 2012, 4, 1233-1238.	4.0	65
141	Hierarchical porous carbon microrods composed of vertically aligned graphene-like nanosheets for Li-ion batteries. Journal of Materials Chemistry A, 2015, 3, 19800-19806.	5.2	62
142	Single-crystalline tin-doped indium oxide whiskers: Synthesis and characterization. Applied Physics Letters, 2004, 85, 4759-4761.	1.5	61
143	Ionic liquid-modulated preparation of hexagonal tungsten trioxide mesocrystals for lithium-ion batteries. Nanoscale, 2015, 7, 2230-2234.	2.8	61
144	3D hierarchical CuO mesocrystals from ionic liquid precursors: towards better electrochemical performance for Li-ion batteries. Journal of Materials Chemistry A, 2016, 4, 8402-8411.	5.2	61

#	Article	IF	CITATIONS
145	Topochemical synthesis of cobalt oxide nanowire arrays for high performance binderless lithium ion batteries. Journal of Materials Chemistry, 2011, 21, 11867.	6.7	60
146	Anomalous conductivity-type transition sensing behaviors of n-type porous α-Fe2O3 nanostructures toward H2S. Materials Science and Engineering B: Solid-State Materials for Advanced Technology, 2011, 176, 600-605.	1.7	60
147	An excellent enzyme biosensor based on Sb-doped SnO2 nanowires. Biosensors and Bioelectronics, 2010, 25, 2436-2441.	5.3	59
148	Catalytic growth of In2O3 nanobelts by vapor transport. Journal of Crystal Growth, 2006, 290, 660-664.	0.7	58
149	High-performance room-temperature hydrogen sensors based on combined effects of Pd decoration and Schottky barriers. Nanoscale, 2013, 5, 2505.	2.8	58
150	Long circulating reduced graphene oxide–iron oxide nanoparticles for efficient tumor targeting and multimodality imaging. Nanoscale, 2016, 8, 12683-12692.	2.8	58
151	The optical properties of ZnO sheets electrodeposited on ITO glass. Materials Letters, 2007, 61, 2000-2003.	1.3	57
152	Designable fabrication of flower-like SnS2 aggregates with excellent performance in lithium-ion batteries. RSC Advances, 2012, 2, 3615.	1.7	57
153	Rational synthesis of ZnMn ₂ O ₄ porous spheres and graphene nanocomposite with enhanced performance for lithium-ion batteries. Journal of Materials Chemistry A, 2015, 3, 11430-11436.	5.2	57
154	Controlled synthesis of iron sulfide coated by carbon layer to improve lithium and sodium storage. Electrochimica Acta, 2017, 247, 1080-1087.	2.6	56
155	Indium-tin-oxide thin film transistor biosensors for label-free detection of avian influenza virus H5N1. Analytica Chimica Acta, 2013, 773, 83-88.	2.6	55
156	Highly sensitive ethanol sensors based on {100}-bounded In2O3 nanocrystals due to face contact. Applied Physics Letters, 2006, 89, 243514.	1.5	54
157	Low-temperature synthesis and electrical transport properties of W18O49 nanowires. Journal of Crystal Growth, 2008, 310, 462-466.	0.7	54
158	Ultrasensitive ethanol sensor based on 3D aloe-like SnO2. Sensors and Actuators B: Chemical, 2012, 166-167, 7-11.	4.0	54
159	Homogenous incorporation of SnO2 nanoparticles in carbon cryogels via the thermal decomposition of stannous sulfate and their enhanced lithium-ion intercalation properties. Nano Energy, 2013, 2, 769-778.	8.2	54
160	Electrospun CeO 2 nanoparticles/PVP nanofibers based high-frequency surface acoustic wave humidity sensor. Sensors and Actuators B: Chemical, 2016, 223, 730-737.	4.0	54
161	Two-Dimensional Single Crystal CdS Nanosheets: Synthesis and Properties. Crystal Growth and Design, 2010, 10, 4995-5000.	1.4	53
162	Hierarchical CuCo ₂ O ₄ nanowire@NiCo ₂ O ₄ nanosheet core/shell arrays for high-performance supercapacitors. RSC Advances, 2015, 5, 69636-69641.	1.7	53

#	Article	IF	CITATIONS
163	Ultrahigh ethanol response of SnO2 nanorods at low working temperature arising from La2O3 loading. Sensors and Actuators B: Chemical, 2009, 140, 426-431.	4.0	52
164	S-doped carbon@TiO2 to store Li+/Na+ with high capacity and long life-time. Energy Storage Materials, 2018, 13, 215-222.	9.5	52
165	Rational design of Au–NiO hierarchical structures with enhanced rate performance for supercapacitors. Journal of Materials Chemistry A, 2013, 1, 7023.	5.2	50
166	Functionalized tetrapod-like ZnO nanostructures for plasmid DNA purification, polymerase chain reaction and delivery. Nanotechnology, 2007, 18, 015101.	1.3	49
167	Photoresponse of SnO2nanobelts grownin situon interdigital electrodes. Nanotechnology, 2007, 18, 285502.	1.3	49
168	Enhanced sensing properties of defect-controlled ZnO nanotetrapods arising from aluminum doping. Sensors and Actuators B: Chemical, 2010, 147, 165-169.	4.0	49
169	Facet-induced formation of hematite mesocrystals with improved lithium storage properties. Chemical Communications, 2012, 48, 12204.	2.2	49
170	Topochemical Synthesis of Cobalt Oxideâ€Based Porous Nanostructures for Highâ€Performance Lithiumâ€Ion Batteries. Chemistry - A European Journal, 2011, 17, 1596-1604.	1.7	48
171	Gram-scale synthesis of ultrasmall SnO2 nanocrystals with an excellent electrochemical performance. Nanoscale, 2013, 5, 3262.	2.8	48
172	Humidity sensing properties of a single Sb doped SnO2 nanowire field effect transistor. Sensors and Actuators B: Chemical, 2013, 186, 78-83.	4.0	48
173	Enhanced H2 gas sensing properties by Pd-loaded urchin-like W18O49 hierarchical nanostructures. Sensors and Actuators B: Chemical, 2018, 260, 900-907.	4.0	48
174	Facile synthesis of flower-like Cu3BiS3 hierarchical nanostructures and their electrochemical properties for lithium-ion batteries. CrystEngComm, 2012, 14, 550-554.	1.3	47
175	Facile Synthesis of Graphene@NiO/MoO3 Composite Nanosheet Arrays for High-performance Supercapacitors. Electrochimica Acta, 2015, 151, 510-516.	2.6	47
176	Ethanol-sensing performance of tin dioxide octahedral nanocrystals with exposed high-energy {111} and {332} facets. Journal of Materials Chemistry A, 2014, 2, 10623.	5.2	46
177	Memory and negative photoconductivity effects of Ge nanocrystals embedded in ZrO2/Al2O3 gate dielectrics. Applied Physics Letters, 2003, 83, 138-140.	1.5	45
178	Large-scale controlled synthesis of silica nanotubes using zinc oxide nanowires as templates. Nanotechnology, 2005, 16, 1978-1982.	1.3	45
179	Electronic transport characteristics through individual ZnSnO3 nanowires. Applied Physics Letters, 2006, 88, 182102.	1.5	45
180	Ionothermal synthesis of aggregated α-Fe2O3 nanoplates and their magnetic properties. Nanoscale, 2011, 3, 4372.	2.8	45

#	Article	IF	CITATIONS
181	Quantum Size Effect on Surface Photovoltage Spectra:Â Alpha-Fe2O3Nanocrystals on the Surface of Monodispersed Silica Microsphere. Journal of Physical Chemistry B, 2006, 110, 7259-7264.	1.2	44
182	Low-temperature sensing and high sensitivity of ZnO nanoneedles due to small size effect. Thin Solid Films, 2009, 517, 5931-5934.	0.8	44
183	Highly chemoresistive humidity sensing using poly(ionic liquid)s. Chemical Communications, 2016, 52, 8417-8419.	2.2	44
184	Fast-response ionogel humidity sensor for real-time monitoring of breathing rate. Materials Chemistry Frontiers, 2019, 3, 484-491.	3.2	43
185	Facile preparation of porous one-dimensional Mn2O3 nanostructures and their application as anode materials for lithium-ion batteries. Physica E: Low-Dimensional Systems and Nanostructures, 2010, 43, 70-75.	1.3	42
186	3-D mesoporous nano/micro-structured Fe3O4/C as a superior anode material for lithium-ion batteries. Journal of Solid State Electrochemistry, 2011, 15, 2563-2569.	1.2	42
187	Synthesis of highly aligned and ultralong coordination polymer nanowires and their calcination to porous manganese oxide nanostructures. Journal of Materials Chemistry, 2012, 22, 4982.	6.7	42
188	Hierarchical SnO2 Nanospheres: Bio-inspired Mineralization, Vulcanization, Oxidation Techniques and the Application for NO Sensors. Scientific Reports, 2013, 3, 3500.	1.6	42
189	Fixing graphene-Mn3O4 nanosheets on carbon cloth by a poles repel-assisted method to prepare flexible binder-free electrodes for supercapacitors. Electrochimica Acta, 2015, 180, 983-989.	2.6	42
190	Comparison of the electrochemical performance of iron hexacyanoferrate with high and low quality as cathode materials for aqueous sodium-ion batteries. Chemical Communications, 2017, 53, 6780-6783.	2.2	42
191	Electrospinning Synthesis of Ni°, Fe° Codoped Ultrafine-ZnFe2O4/C Nanofibers and Their Properties for Lithium Ion Storage. Electrochimica Acta, 2016, 194, 357-366.	2.6	41
192	Chemical bath deposition of SnS2 nanowall arrays with improved electrochemical performance for lithium ion battery. Materials Letters, 2010, 64, 2350-2353.	1.3	40
193	Encapsulating Sn _{<i>x</i>} Sb Nanoparticles in Multichannel Graphene-Carbon Fibers As Flexible Anodes to Store Lithium Ions with High Capacities. ACS Applied Materials & Interfaces, 2015, 7, 21890-21897.	4.0	40
194	MOF-derived porous ZnO/ZnFe 2 O 4 hybrid nanostructures as advanced anode materials for lithium ion batteries. Materials Letters, 2017, 197, 241-244.	1.3	40
195	Sâ€Doped Carbon Fibers Uniformly Embedded with Ultrasmall TiO ₂ for Na ⁺ /Li ⁺ Storage with High Capacity and Longâ€Time Stability. Small, 2019, 15, e1902201.	5.2	40
196	Individual core-shell structured ZnSnO3 nanowires as photoconductors. Materials Letters, 2008, 62, 1356-1358.	1.3	39
197	Temperature-Dependent Abnormal and Tunable p-n Response of Tungsten Oxide–Tin Oxide Based Gas Sensors. ACS Applied Materials & Interfaces, 2015, 7, 24887-24894.	4.0	39
198	Electric-field-aligned vertical growth and field emission properties of In2O3 nanowires. Applied Physics Letters, 2005, 87, 143104.	1.5	38

#	Article	IF	CITATIONS
199	Simple fabrication of a sensitive hydrogen peroxide biosensor using enzymes immobilized in processable polyaniline nanofibers/chitosan film. Materials Science and Engineering C, 2009, 29, 1794-1797.	3.8	38
200	A novel non-enzymatic hydrogen peroxide sensor based on Mn-nitrilotriacetate acid (Mn-NTA) nanowires. Talanta, 2010, 81, 727-731.	2.9	38
201	Morphology effect on the performances of SnO2 nanorod arrays as anodes for Li-ion batteries. Materials Letters, 2011, 65, 1154-1156.	1.3	38
202	NiMoO ₄ nanowire @ MnO ₂ nanoflake core/shell hybrid structure aligned on carbon cloth for high-performance supercapacitors. RSC Advances, 2015, 5, 10681-10687.	1.7	37
203	Ultralow threshold field emission from ZnO nanorod arrays grown on ZnO film at low temperature. Nanotechnology, 2007, 18, 355606.	1.3	35
204	Vapor phase growth and optical properties of single-crystalline SnO2 nanobelts. Materials Research Bulletin, 2008, 43, 836-842.	2.7	35
205	Ammonia gas detection based on polyaniline nanofibers coated on interdigitated array electrodes. Journal of Materials Science: Materials in Electronics, 2011, 22, 418-421.	1.1	35
206	Rational combination of α-MnS/rGO nanocomposites for high-performance lithium-ion batteries. CrystEngComm, 2016, 18, 6200-6204.	1.3	35
207	Functionalized horizontally aligned CNT array and random CNT network for CO2 sensing. Carbon, 2017, 117, 263-270.	5.4	35
208	Surfactant-Assisted Synthesis of High Energy {010} Facets Beneficial to Li-Ion Transport Kinetics with Layered LiNi _{0.6} Co _{0.2} Mn _{0.2} O ₂ . ACS Sustainable Chemistry and Engineering, 2018, 6, 6312-6320.	3.2	35
209	Electrospun Li ₃ V ₂ (PO ₄) ₃ nanocubes/carbon nanofibers as free-standing cathodes for high-performance lithium-ion batteries. Journal of Materials Chemistry A, 2019, 7, 14681-14688.	5.2	35
210	Current saturation in multiwalled carbon nanotubes by large bias. Applied Physics Letters, 2004, 84, 3379-3381.	1.5	34
211	A novel preparation and surface decorated approach for α-Fe nanoparticles by chemical vapor–liquid reaction at low temperature. Materials Letters, 2004, 58, 1481-1484.	1.3	34
212	A Phaseâ€Separation Route to Synthesize Porous CNTs with Excellent Stability for Na ⁺ Storage. Small, 2017, 13, 1604045.	5.2	34
213	The full gradient design in Li-rich cathode for high performance lithium ion batteries with reduced voltage decay. Journal of Power Sources, 2019, 437, 226902.	4.0	34
214	Electrocatalytic activity of horseradish peroxidase/chitosan/carbon microsphere microbiocomposites to hydrogen peroxide. Talanta, 2008, 77, 37-41.	2.9	33
215	Facile synthesis of 3D flowerlike α-FeOOH architectures and their conversion into mesoporous α-Fe2O3 for gas-sensing application. Solid State Sciences, 2010, 12, 2125-2129.	1.5	33
216	Hierarchical SnO ₂ Nanostructures: Linear Assembly of Nanorods on the Nanowire Backbones. Journal of Physical Chemistry C, 2010, 114, 1844-1848.	1.5	33

#	Article	IF	CITATIONS
217	Stannous ions reducing graphene oxide at room temperature to produce SnO _x -porous, carbon-nanofiber flexible mats as binder-free anodes for lithium-ion batteries. Journal of Materials Chemistry A, 2015, 3, 12672-12679.	5.2	33
218	Synthesis and electron storage characteristics of isolated silver nanodots on/embedded in Al2O3 gate dielectric. Applied Surface Science, 2004, 230, 8-11.	3.1	32
219	Stimulated emission from trapped excitons in SnO2 nanowires. Physica E: Low-Dimensional Systems and Nanostructures, 2007, 39, 223-229.	1.3	32
220	A nanocomposite of tin dioxide octahedral nanocrystals exposed to high-energy facets anchored onto graphene sheets for high performance lithium-ion batteries. Journal of Materials Chemistry A, 2014, 2, 13990.	5.2	32
221	A facile method to hunt for durable high-rate capability Na0.44MnO2. Journal of Power Sources, 2018, 395, 395-402.	4.0	32
222	Photoluminescence and photosensitive properties of ZnO strands self-twined by nanowires. Nanotechnology, 2004, 15, 559-561.	1.3	31
223	Metal-Organic Frameworks Derived Nanocomposites of Mixed-Valent MnO Nanoparticles In-Situ Grown on Ultrathin Carbon Sheets for High-Performance Supercapacitors and Lithium-Ion Batteries. Electrochimica Acta, 2017, 256, 63-72.	2.6	31
224	Hydrothermal synthesis of α-Ni(OH)2 and its conversion to NiO with electrochemical properties. Journal of Alloys and Compounds, 2014, 582, 328-333.	2.8	30
225	Linear and third-order nonlinear optical absorption of amorphous Ge nanoclusters embedded in Al2O3 matrix synthesized by electron-beam coevaporation. Applied Physics Letters, 2003, 82, 3162-3164.	1.5	29
226	Synthesis and optical properties of semiconducting beta-FeSi2 nanocrystals. Applied Physics Letters, 2003, 82, 3224-3226.	1.5	29
227	Growth of Oriented Zinc Oxide Nanowire Array into Novel Hierarchical Structures in Aqueous Solutions. Journal of Physical Chemistry C, 2008, 112, 17546-17553.	1.5	29
228	Degenerate doping induced metallic behaviors in ZnO nanobelts. Applied Physics Letters, 2008, 93, .	1.5	29
229	ZnO-carbon nanofibers for stable, high response, and selective H ₂ S sensors. Nanotechnology, 2018, 29, 275501.	1.3	29
230	Rapid synthesis of Cr-doped γ-Fe2O3/reduced graphene oxide nanocomposites as high performance anode materials for lithium ionÂbatteries. Journal of Alloys and Compounds, 2018, 732, 270-279.	2.8	29
231	A highly selective and sensitive H ₂ S sensor at low temperatures based on Cr-doped α-Fe ₂ O ₃ nanoparticles. RSC Advances, 2019, 9, 4150-4156.	1.7	29
232	Resonant tunneling of Si nanocrystals embedded in Al2O3 matrix synthesized by vacuum electron-beam co-evaporation. Applied Physics Letters, 2002, 81, 538-540.	1.5	28
233	Ohmic contact junction of carbon nanotubes fabricated byin situelectron beam deposition. Nanotechnology, 2006, 17, 6011-6015.	1.3	28
234	In situ synthesis of In2O3 nanowires with different diameters from indium film. Applied Physics Letters, 2006, 88, 193119.	1.5	28

#	Article	IF	CITATIONS
235	Tin dioxide dodecahedral nanocrystals anchored on graphene sheets with enhanced electrochemical performance for lithium-ion batteries. Electrochimica Acta, 2015, 159, 46-51.	2.6	28
236	The effect of loading density of nickel-cobalt sulfide arrays on their cyclic stability and rate performance for supercapacitors. Science China Materials, 2016, 59, 629-638.	3.5	28
237	Electrospun Nb-doped LiNi _{0.4} Co _{0.2} Mn _{0.4} O ₂ nanobelts for lithium-ion batteries. Inorganic Chemistry Frontiers, 2018, 5, 1126-1132.	3.0	28
238	Prostate Specific Antigen Detection Using Microgapped Electrode Array Immunosensor with Enzymatic Silver Deposition. Clinical Chemistry, 2009, 55, 964-971.	1.5	27
239	Improvement of electron transport in a ZnSe nanowire by in situ strain. Journal Physics D: Applied Physics, 2011, 44, 125301.	1.3	27
240	Sulfated mesoporous Au/TiO2 spheres as a highly active and stable solid acid catalyst. Journal of Materials Chemistry, 2012, 22, 13216.	6.7	27
241	Preparation and magnetic properties of CoWO ₄ nanocrystals. Crystal Research and Technology, 2012, 47, 1004-1007.	0.6	27
242	Reduced graphene oxide uniformly anchored with ultrafine CoMn 2 O 4 nanoparticles as advance anode materials for lithium and sodium storage. Journal of Alloys and Compounds, 2017, 716, 30-36.	2.8	27
243	A layer-by-layer deposition strategy of fabricating NiO@rGO composites for advanced electrochemical capacitors. Electrochimica Acta, 2015, 152, 378-382.	2.6	26
244	Multifunctional Cr 2 O 3 quantum nanodots to improve the lithium-ion storage performance of free-standing carbon nanofiber networks. Electrochimica Acta, 2016, 217, 55-61.	2.6	26
245	In-situ phase transition to form porous h-MoO3@C nanofibers with high stability for Li+/Na+ storage. Science China Materials, 2017, 60, 755-765.	3.5	25
246	Octopus tentacles-like WO3/C@CoO as high property and long life-time electrocatalyst for hydrogen evolution reaction. Electrochimica Acta, 2018, 281, 1-8.	2.6	25
247	In-situ fabrication of reduced graphene oxide (rGO)/ZnO heterostructure: surface functional groups induced electrical properties. Electrochimica Acta, 2016, 196, 558-564.	2.6	24
248	Abnormal temperature dependence of conductance of single Cd-doped ZnO nanowires. Applied Physics Letters, 2005, 86, 263101.	1.5	23
249	Facile approach to prepare porous GeO2/SnO2 nanofibers via a single spinneret electrospinning technique as anodes for Lithium-ion batteries. Ceramics International, 2015, 41, 10308-10313.	2.3	23
250	Stable electron field emission from triangular-shaped ZnO nanoplate arrays with low local heating effects. Nanotechnology, 2007, 18, 165704.	1.3	22
251	Tailoring the subunits of α-Fe2O3 nanoplates for optimizing electrochemical performance. Electrochimica Acta, 2013, 113, 194-199.	2.6	22
252	Surrounding Sensitive Electronic Properties of Bi2Te3 Nanoplates—Potential Sensing Applications of Topological Insulators. Scientific Reports, 2014, 4, 4639.	1.6	22

#	Article	IF	CITATIONS
253	Gas modulating effect in room temperature ammonia sensing. Sensors and Actuators B: Chemical, 2017, 242, 404-411.	4.0	22
254	Sub-band-gap photoconductivity of individual α-Si ₃ N ₄ nanowires. Nanotechnology, 2007, 18, 325603.	1.3	21
255	Fe3O4 dendrites reduced by carbon-coatings as high reversible capacity anodes for lithium ion batteries. Solid State Sciences, 2010, 12, 2024-2029.	1.5	21
256	Enhanced sensitivity of a GHz surface acoustic wave humidity sensor based on Ni(SO ₄) _{0.3} (OH) _{1.4} nanobelts and NiO nanoparticles. Journal of Materials Chemistry C, 2015, 3, 9902-9909.	2.7	21
257	Ultra-fast and highly-sensitive gas sensing arising from thin SnO2 inner wall supported hierarchical bilayer oxide hollow spheres. Sensors and Actuators B: Chemical, 2017, 240, 349-357.	4.0	21
258	Room-temperature H2 sensing interfered by CO based on interfacial effects in palladium-tungsten oxide nanoparticles. Sensors and Actuators B: Chemical, 2018, 254, 966-972.	4.0	21
259	Mesoporous SnO2 nanospheres formed via a water-evaporating process with superior electrochemical properties. CrystEngComm, 2012, 14, 6170.	1.3	20
260	Non-enzymatic electrochemical glucose sensor based on NiMoO ₄ nanorods. Nanotechnology, 2015, 26, 145501.	1.3	20
261	Construction of complex WO3-SnO2 hollow nanospheres as a high-performance anode for lithium-ion batteries. Journal of Alloys and Compounds, 2018, 744, 375-380.	2.8	20
262	Thin film transistors fabricated by in situ growth of SnO2 nanobeltson Auâ^•Pt electrodes. Applied Physics Letters, 2004, 85, 1805-1807.	1.5	19
263	Design and synthesis of Cr2O3@C@G composites with yolk-shell structure for Li+ storage. Journal of Alloys and Compounds, 2017, 724, 406-412.	2.8	19
264	Oxygen vacancy improves the hydrogen evolution reaction property of WO <mml:math xmlns:mml="http://www.w3.org/1998/Math/MathML" id="mml14" display="inline" overflow="scroll" altimg="si14.gif"><mml:msub><mml:mrow /><mml:mrow><mml:mn>3</mml:mn><mml:mo>a^2</mml:mo><mml:mi>x</mml:mi></mml:mrow></mml:mrow </mml:msub></mml:math 	1.9 <td>19 th></td>	19 th>
265	nanosheets. Nano Structures Nano Objects, 2018, 15, 114-118. Third-order optical nonlinearity and negative photoconductivity of Ge nanocrystals in Al2O3dielectric. Nanotechnology, 2003, 14, L15-L17.	1.3	18
266	l–Vcharacteristics of Schottky contacts of semiconducting ZnSe nanowires and gold electrodes. Nanotechnology, 2006, 17, 2420-2423.	1.3	18
267	Amorphous SnO2–SiO2 thin films with reticular porous morphology for lithium-ion batteries. Applied Physics Letters, 2008, 93, .	1.5	18
268	High surface-enhanced Raman scattering activity from Au-decorated individual and branched tin oxide nanowires. Journal of Applied Physics, 2009, 106, .	1.1	17
269	Seed-free, aqueous synthesis of gold nanowires. CrystEngComm, 2012, 14, 7549.	1.3	17
270	Hierarchical tin-based microspheres: Solvothermal synthesis, chemical conversion, mechanism and application in lithium ion batteries. Electrochimica Acta, 2013, 106, 386-391.	2.6	17

#	Article	IF	CITATIONS
271	Giant Thermopower of Hydrogen Ion Enhanced by a Strong Hydrogen Bond System. ACS Applied Materials & Interfaces, 2022, 14, 19304-19314.	4.0	17
272	Observation of surface structural changes of Pt octahedron nanoparticles and its effect in electrocatalysis oxidation of methanol. Catalysis Communications, 2009, 10, 1244-1247.	1.6	16
273	Mismatch and chemical composition analysis of vertical InxGa1â^'xAs quantum-dot arrays by transmission electron microscopy. Applied Physics Letters, 2001, 78, 3830-3832.	1.5	15
274	Titanium-induced germanium nanocones synthesized by vacuum electron-beam evaporation: growth mechanism and morphology evolution. Solid State Communications, 2003, 125, 503-507.	0.9	15
275	The large-scale synthesis of one-dimensional TiO ₂ nanostructures using palladium as catalyst at low temperature. Nanotechnology, 2009, 20, 055605.	1.3	15
276	H x MoO 3 nanobelts with better performance as anode in lithium-ion batteries. Electrochimica Acta, 2016, 213, 641-647.	2.6	15
277	Synthesis of electrocatalytically functional carbon honeycombs through cooking with molecule precursors. International Journal of Hydrogen Energy, 2017, 42, 6472-6481.	3.8	15
278	3D reticular pomegranate-like CoMn 2 O 4 /C for ultrahigh rate lithium-ion storage with re-oxidation of manganese. Electrochimica Acta, 2017, 241, 244-251.	2.6	15
279	Non-Contact and Non-Destructive Measurement of Carrier Concentration of Nitrogen-Doped ZnSe by Reflectance Difference Spectroscopy. Japanese Journal of Applied Physics, 1997, 36, 6638-6644.	0.8	14
280	A netlike DNA-templated Au nanoconjugate as the matrix of the direct electrochemistry of horseradish peroxidase. Electrochemistry Communications, 2009, 11, 327-330.	2.3	14
281	Small quantities of cobalt deposited on tin oxide as anode material to improve performance of lithium-ion batteries. Nanoscale, 2012, 4, 5731.	2.8	14
282	High-vacuum electron-beam co-evaporation of Si nanocrystals embedded in Al2O3 matrix. Applied Surface Science, 2002, 191, 171-175.	3.1	13
283	The synthesis and photoluminescence of multipod-like zinc oxide whiskers. Journal of Physics Condensed Matter, 2004, 16, 1115-1121.	0.7	13
284	Electrospinning–thermal treatment synthesis: a general strategy to decorate highly porous nanotubes on both internal and external side-walls with metal oxide/noble metal nanoparticles. Nanoscale, 2013, 5, 2835.	2.8	13
285	Hysteresis in current transport in a GaAs diode containing self-assembled InAs quantum dots. Applied Physics A: Materials Science and Processing, 2001, 73, 615-619.	1.1	12
286	Ultra-high-density Ge quantum dots on insulator prepared by high-vacuum electron-beam evaporation. Journal of Crystal Growth, 2003, 249, 23-27.	0.7	12
287	Carbon Nanotube Radio-Frequency Single-Electron Transistor. Journal of Low Temperature Physics, 2004, 136, 465-480.	0.6	12
288	Large optical third-order nonlinearity of composite thin film of carbon nanotubes and BaTiO3. Chemical Physics Letters, 2005, 407, 397-401.	1.2	12

#	Article	IF	CITATIONS
289	Strongly coupled hybrid nanostructures for selective hydrogen detection – understanding the role of noble metals in reducing cross-sensitivity. Nanoscale, 2014, 6, 4758-4764.	2.8	12
290	Architectures of tavorite LiFe(PO ₄)(OH) _{0.5} F _{0.5} hierarchical microspheres and their lithium storage properties. Nanoscale, 2014, 6, 11041-11045.	2.8	12
291	New Insights on the Fast Response of Poly(Ionic Liquid)s to Humidity: The Effect of Free-Ion Concentration. Nanomaterials, 2019, 9, 749.	1.9	12
292	A double-walled carbon nanotube field-effect transistor using the inner shell as its gate. Physica E: Low-Dimensional Systems and Nanostructures, 2004, 23, 232-236.	1.3	11
293	Setup for shot noise measurements in carbon nanotubes. AIP Conference Proceedings, 2006, , .	0.3	11
294	High-performance humidity sensors from Ni(SO ₄) _{0.3} (OH) _{1.4} nanobelts. Nanoscale, 2014, 6, 6521-6525.	2.8	11
295	LiFePO4mesocrystals coated with N-doped carbon from an ionic liquid for Li-ion batteries. CrystEngComm, 2017, 19, 1253-1257.	1.3	11
296	Aggregating complementary boundary contrast with smoothing for salient region detection. Visual Computer, 2017, 33, 1155-1167.	2.5	11
297	In2O3 nanowires grown from Auâ^In film on glass. Applied Physics Letters, 2006, 88, 163111.	1.5	10
298	Rational design and synthesis of sandwich-like iron nitride-graphene composites as efficient catalysts for oxygen reduction reaction. International Journal of Hydrogen Energy, 2017, 42, 202-211.	3.8	10
299	A free-standing Li _{1.2} Mn _{0.54} Ni _{0.13} Co _{0.13} O ₂ /MWCNT framework for high-energy lithium-ion batteries. Inorganic Chemistry Frontiers, 2018, 5, 3053-3060.	3.0	10
300	General Airbrushâ€Spraying/Electrospinning Strategy for Ultrahigh Arealâ€Capacity LiFePO ₄ â€Based Cathodes. ChemElectroChem, 2018, 5, 2330-2335.	1.7	10
301	Si single-electron transistors with in-plane point-contact metal gates. Applied Physics Letters, 2001, 78, 2160-2162.	1.5	9
302	In situ growth of nanowire on the tip of a carbon nanotube under strong electric field. Applied Physics Letters, 2005, 86, 133103.	1.5	9
303	Synthesis of vertically electric-field-aligned In2O3 nanowires. Materials Letters, 2006, 60, 1492-1495.	1.3	9
304	Electrografted Poly(<i>N</i> â€mercaptoethyl acrylamide) and Au Nanoparticlesâ€Based Organic/Inorganic Film: A Platform for the Highâ€Performance Electrochemical Biosensors. Chemistry - an Asian Journal, 2010, 5, 919-924.	1.7	9
305	Typeâ€&witchable Inverter and Amplifier Based on Highâ€Performance Ambipolar Blackâ€Phosphorus Transistors. Advanced Electronic Materials, 2019, 5, 1900133.	2.6	9
306	CeO2/ionic liquid hybrid materials with enhanced humidity performance. Sensors and Actuators B: Chemical, 2017, 252, 870-876.	4.0	8

#	Article	IF	CITATIONS
307	Energy Storage: A Phase-Separation Route to Synthesize Porous CNTs with Excellent Stability for Na ⁺ Storage (Small 22/2017). Small, 2017, 13, .	5.2	8
308	Characteristics of a field-effect transistor with stacked InAs quantum dots. Applied Physics Letters, 2003, 82, 3092-3094.	1.5	7
309	Self-assembled Au–Si alloy nanocones: synthesis and electron field emission characteristics. Applied Surface Science, 2004, 221, 38-42.	3.1	7
310	Vapor Phase Growth of ZnO Nanorod–Nanobelt Junction Arrays. Journal of Nanoscience and Nanotechnology, 2005, 5, 1120-1124.	0.9	7
311	Currentâ^'Voltage Characteristics of in Situ Graphitization of Hydrocarbon Coated on ZnSe Nanowire. Journal of Physical Chemistry C, 2010, 114, 12839-12849.	1.5	7
312	Solvothermal Synthesis of Hollow Urchin-Like SnO2 Nanospheres with Superior Lithium Storage Behavior. Journal of Nanoscience and Nanotechnology, 2013, 13, 4297-4301.	0.9	7
313	Ionic liquid-assisted fabrication of copper hydroxyphosphate nanocrystals with exposed {100} facets for enhanced photocatalytic activity. Nanotechnology, 2015, 26, 031001.	1.3	7
314	Janus particle-based microprobes: Determination of object orientation. Colloids and Surfaces A: Physicochemical and Engineering Aspects, 2017, 513, 452-462.	2.3	7
315	Synthesis and Characterization of Hydrocarbon Coating Prepared by in Situ Electron Beam Deposition on ZnSe Nanowire. Journal of Physical Chemistry C, 2008, 112, 7572-7578.	1.5	6
316	Edge-truncated cubic platinum nanoparticles as anode catalysts for direct methanol fuel cells. Applied Physics Letters, 2008, 92, .	1.5	6
317	Growth of flower-like CdSe dendrites from a BrÃ,nsted acid–base ionic liquid precursor. RSC Advances, 2012, 2, 5944.	1.7	6
318	Muti-component nanocomposite of nickel and manganese oxides with enhanced stability and catalytic performance for non-enzymatic glucose sensors. Nanotechnology, 2016, 27, 255501.	1.3	6
319	Single-electron charging in a parallel dot structure. Applied Physics Letters, 2001, 78, 634-636.	1.5	5
320	Single-electron transistors with point contact channels. Nanotechnology, 2002, 13, 221-225.	1.3	5
321	Transport through a Si single-electron transistor. Physica B: Condensed Matter, 2001, 301, 169-173.	1.3	4
322	Fast Response Amperometric Biosensor for H ₂ O ₂ Detection Based on Horseradish-Peroxidase/Titania-Nanowires/Chitosan Modified Glassy Carbon Electrode. Sensor Letters, 2009, 7, 543-549.	0.4	4
323	Design and fabrication of a three modules micro smart qPCR system. , 2009, , .		3
324	Amorphous tin–iron oxide thin films with 3D reticular porous morphology for lithiumâ€ion batteries. Crystal Research and Technology, 2013, 48, 51-54.	0.6	3

#	Article	IF	CITATIONS
325	Lithium battery swollen detection based on computer vision. , 2013, , .		3
326	Coulomb blockade oscillations of si single-electron transistors. Chinese Physics B, 2001, 10, 844-846.	1.3	2
327	Electrodeposition of aligned ZnO sheet array on ITO substrate and their field emission characteristics. Chinese Physics B, 2007, 16, 3545-3548.	1.3	2
328	Evaporation Phenomenon in Micro Polymerase Chain Reaction (μPCR) System and a Possible Electrowetting Solution. Journal of Adhesion Science and Technology, 2012, 26, 2125-2134.	1.4	2
329	Reprint of "A layer-by-layer deposition strategy of fabricating NiO@rGO composites for advanced electrochemical capacitors― Electrochimica Acta, 2015, 172, 37-41.	2.6	2
330	The Improvement of SiO2 Nanoparticles on the Oxygen Reduction Reaction Property of Nitrogen-Doped Mesoporous Graphene Spheres Prepared by Spray Drying. Nanoscience and Nanotechnology Letters, 2018, 10, 200-206.	0.4	2
331	Classification of Cognitive Impairment and Healthy Controls Based on Transcranial Magnetic Stimulation Evoked Potentials. Frontiers in Aging Neuroscience, 2021, 13, 804384.	1.7	2
332	Etching trenches to effectively create electron quantum wires for single-electron-transistor applications. Applied Physics Letters, 2001, 78, 3705-3707.	1.5	1
333	One-pot synthesis of crystalline SnO2 nanoparticles and their low-temperature ethanol sensing characteristics. Science in China Series G: Physics, Mechanics and Astronomy, 2009, 52, 1601-1605.	0.2	1
334	Application of computational verb theory to gas recognition. , 2012, , .		1
335	Sonochemical Synthesis, Optical Properties, and Electrical Properties of Core/Shell-Typ ZnO Nanorod/CdS Nanoparticle Composites ChemInform, 2005, 36, no.	0.1	0
336	A modified attribute reduction algorithm of consistent covering decision information systems. , 2012, , .		0
337	Metal Oxide Nanowire Sensors with Complex Morphologies and Compositions. , 2013, , 345-364.		0
338	Security evaluation of RC4 using big data analytics. , 2016, , .		0
339	A Hybrid Chemical Reaction Optimization Algorithm for Bin Packing Problem. , 2017, , .		0
340	Na/Liâ€lon Batteries: Sâ€Doped Carbon Fibers Uniformly Embedded with Ultrasmall TiO ₂ for Na ⁺ /Li ⁺ Storage with High Capacity and Longâ€Time Stability (Small 38/2019). Small, 2019, 15, 1970207.	5.2	0
341	Rapid Pedestrian Detection Based On Movement Trend. , 2016, , .		0
342	Moving Pedestrian Detection Using Normed Proposals and Key Points Matching. , 2016, , .		0

Moving Pedestrian Detection Using Normed Proposals and Key Points Matching. , 2016, , . 342